

Quantum Error Mitigation using Symmetry Expansion

Zhenyu Cai*

Department of Materials, University of Oxford, Oxford, OX1 3PH, United Kingdom

(Dated: March 2, 2022)

Even with the recent rapid developments in quantum hardware, noise remains the biggest challenge for the practical applications of any near-term quantum devices. Full quantum error correction cannot be implemented in these devices due to their limited scale. Therefore instead of relying on engineered code symmetry, symmetry verification was developed which uses the inherent symmetry within the physical problem we try to solve. In this article, we develop a general framework named symmetry expansion which provides a wide spectrum of symmetry-based error mitigation schemes beyond symmetry verification, enabling us to achieve different balances between the errors in the result and the sampling cost of the scheme. We show a way to identify a near-optimal symmetry expansion scheme that could achieve much lower errors than symmetry verification. By numerically simulating the Fermi-Hubbard model for energy estimation, the near-optimal symmetry expansion can achieve estimation errors 6 to 9 times below what is achievable by symmetry verification when the average number of circuit errors is between 1 to 2. The corresponding sampling cost for shot noise reduction is just 2 to 6 times higher than symmetry verification. Beyond symmetries inherent to the physical problem, our formalism is also applicable to engineered symmetries. For example, the recent scheme for exponential error suppression using multiple noisy copies of the quantum device is just a special case of symmetry expansion using the permutation symmetry among the copies.

I. INTRODUCTION

The ultimate goal of implementing a fully fault-tolerant quantum error correction scheme for quantum algorithms with provable speed-up may still be years away. However, the recent rapid advance in quantum computing hardware has enabled certain computational tasks to be performed that are well beyond classical capabilities [1, 2], prompting the question of whether it is possible to perform any practically useful tasks with the noisy intermediate-scale quantum (NISQ) devices that we will soon have.

One of the biggest roadblocks for such a goal is how to alleviate the damage done by the noise in these NISQ devices with the limited quantum resource we have. This brings us to *quantum error mitigation*, which unlike quantum error correction, mostly relies on performing additional measurements instead of employing additional qubits to mitigate the damages caused by errors [3–6]. *Symmetry verification* is one such technique which projects the noisy output quantum state back into the symmetry subspace defined by the physical problem we try to solve [7, 8]. Besides measuring all symmetries in every circuit run and discarding the runs that fail any symmetry test, symmetry verification can also be carried out in a post-processing way with a much simpler measurement scheme inspired by quantum subspace expansion [7, 9]. Since stabiliser code decoding can be viewed as symmetry verification with engineered symmetry, we can also apply similar post-processing techniques to reduce the practical challenges in the stabiliser code implementation [10].

More recently, two teams have independently developed a quantum error mitigation scheme that uses multiple copies of the noisy quantum device to suppress errors exponentially as the number of copies increases [11, 12]. The method was named *virtual distillation* by one of the teams. Its core idea relies on the permutation symmetry among the copies, but the way it is implemented does not involve projecting the noisy state into the correct symmetry subspace, and thus does not fall within the symmetry verification framework. In fact, the corresponding permutation symmetry verification [13–15] can only suppress errors linearly with the increase of the number of copies instead of exponentially.

In this article, we will provide a general framework named *symmetry expansion* that encompasses a much wider range of symmetry-based error mitigation schemes beyond symmetry verification. We will discuss ways to search within this wide range of symmetry expansion schemes and identify one that can outperform symmetry verification, just as virtual distillation arises from the permutation symmetry group and vastly outperform the permutation symmetry verification.

We will start by introducing the framework of symmetry expansion in Section II, then we will outline the way to identify a good symmetry expansion scheme in Section III. Moving onto Section IV, we will focus on the implementation of symmetry expansion for Pauli symmetry. In the end, we will finish with an explicit numerical example for the application of symmetry expansion in Section V, along with the conclusion and outlook in Section VI.

* cai.zhenyu.physics@gmail.com

II. SYMMETRY EXPANSION

We are given a circuit that would ideally generate the noiseless state $|\psi_0\rangle$ which is stabilised by a group of symmetry operations \mathbb{G} :

$$G|\psi_0\rangle = |\psi_0\rangle \quad \forall G \in \mathbb{G}.$$

The symmetry subspace $\mathcal{V}_{\mathbb{G}}$ that $|\psi_0\rangle$ lives in, within which all $G \in \mathbb{G}$ will act trivially, is defined by the projector [16]:

$$\Pi_{\mathbb{G}} = \frac{1}{|\mathbb{G}|} \sum_{G \in \mathbb{G}} G. \quad (1)$$

By definition we have

$$\Pi_{\mathbb{G}}^\dagger = \Pi_{\mathbb{G}}, \quad \Pi_{\mathbb{G}} |\psi_0\rangle = |\psi_0\rangle. \quad (2)$$

In reality, the output of the circuit is a noisy state ρ that might have components outside the symmetry subspace. Hence, we will project ρ back into the symmetry subspace $\mathcal{V}_{\mathbb{G}}$ to mitigate the damage of the noise and we will call this process *symmetry verification* [7, 8]. The effective density matrix we obtain after symmetry verification is simply:

$$\rho_{sym} = \frac{\Pi_{\mathbb{G}} \rho \Pi_{\mathbb{G}}}{\text{Tr}(\Pi_{\mathbb{G}} \rho)} = \frac{\Pi_{\mathbb{G}} \rho \Pi_{\mathbb{G}}}{\langle \Pi_{\mathbb{G}} \rangle}. \quad (3)$$

Throughout this article, we will use $\langle O \rangle = \text{Tr}(O\rho)$ to denote the expectation value of some observable O from the *noisy* circuit. Using Eq. (3), the expectation value of some observable O after symmetry verification will be:

$$\text{Tr}(O\rho_{sym}) = \frac{\text{Tr}(O\Pi_{\mathbb{G}}\rho\Pi_{\mathbb{G}})}{\langle \Pi_{\mathbb{G}} \rangle} = \frac{\langle \Pi_{\mathbb{G}} O \Pi_{\mathbb{G}} \rangle}{\langle \Pi_{\mathbb{G}} \rangle}. \quad (4)$$

In *direct symmetry verification*, we will measure the observable O and the symmetry verification result $\Pi_{\mathbb{G}}$ in the same circuit run and discard the circuit runs that fail the symmetry test ($\Pi_{\mathbb{G}} = 0$). This would require

$$[O, \Pi_{\mathbb{G}}] = 0 \quad (5)$$

and thus we have:

$$\text{Tr}(O\rho_{sym}) = \frac{\text{Tr}(O\Pi_{\mathbb{G}}\rho)}{\langle \Pi_{\mathbb{G}} \rangle} = \frac{\langle O\Pi_{\mathbb{G}} \rangle}{\langle \Pi_{\mathbb{G}} \rangle}. \quad (6)$$

Alternatively, Eq. (6) will also hold if we have

$$[\rho, \Pi_{\mathbb{G}}] = 0. \quad (7)$$

How this may arise will be further discussed in Section III C. Note that the normalisation factor $\langle \Pi_{\mathbb{G}} \rangle$ is essentially the fraction of circuit runs that pass the symmetry verification.

We can also apply symmetry verification in a *post-processing* way. Using Eq. (1), we see that we can actually obtain $\langle \Pi_{\mathbb{G}} \rangle$ by uniformly sampling from random

$G \in \mathbb{G}$. Similarly, we can also obtain $\langle O\Pi_{\mathbb{G}} \rangle$ by uniformly sampling from random OG for $G \in \mathbb{G}$. In each circuit run, if we measure O along with a random $G \in \mathbb{G}$, we can compose them to obtain both G and OG and thus effectively obtaining samples for $\langle \Pi_{\mathbb{G}} \rangle$ and $\langle O\Pi_{\mathbb{G}} \rangle$, which in turn can give us the estimate of $\text{Tr}(O\rho_{sym})$ via Eq. (6).

Instead of sampling uniformly from \mathbb{G} , we can sample each symmetry G with the weight w_G , and we will call this more general sampling scheme *symmetry expansion*. By denoting the sampling weight distribution as \vec{w} , the resultant observable following our new sampling scheme will be:

$$\text{Tr}(O\rho_{\vec{w}}) = \frac{\text{Tr}(O\Gamma_{\vec{w}}\rho)}{\text{Tr}(\Gamma_{\vec{w}}\rho)} = \frac{\langle O\Gamma_{\vec{w}} \rangle}{\langle \Gamma_{\vec{w}} \rangle} \quad (8)$$

where $\Gamma_{\vec{w}}$ is the *symmetry expansion operator*:

$$\Gamma_{\vec{w}} = \frac{\sum_{G \in \mathbb{G}} w_G G}{\sum_{G \in \mathbb{G}} w_G} \quad (9)$$

and $\rho_{\vec{w}}$ is the symmetry-expanded ‘density operator’:

$$\rho_{\vec{w}} = \frac{\Gamma_{\vec{w}}\rho}{\text{Tr}(\Gamma_{\vec{w}}\rho)} = \frac{\Gamma_{\vec{w}}\rho}{\langle \Gamma_{\vec{w}} \rangle}. \quad (10)$$

The symmetry expansion operation acting on ρ here is not a completely positive map and thus $\rho_{\vec{w}}$ is not necessarily a valid density operator in the usual sense.

Note that $\Gamma_{\vec{w}}$ is also a symmetry operation:

$$\Gamma_{\vec{w}} |\psi_0\rangle = |\psi_0\rangle. \quad (11)$$

From the definition above we have:

$$\rho_{sym} \equiv \rho_{\vec{1}}, \quad \Pi_{\mathbb{G}} = \Gamma_{\vec{1}}. \quad (12)$$

i.e. symmetry verification is just symmetry expansion with a uniform sampling scheme.

All the sampling weights w_G are by definition positive. Throughout this article we will focus on the case where $\langle G \rangle$ are all real, which would be the case for example when G are all Hermitian. Consequently, $\langle \Gamma_{\vec{w}} \rangle$ will also all be real. Since G are all unitary, we have $-1 \leq \langle G \rangle \leq 1$ for all G , which implies $-1 \leq \langle \Gamma_{\vec{w}} \rangle \leq 1$.

As discussed in Refs. [7, 10], symmetry verification is just a special case of quantum subspace expansion [9]. Assuming all symmetry operators $G \in \mathbb{G}$ commute with the observable O or the noisy state ρ (a special case of Eq. (5) and Eq. (7)), we can see that quantum subspace expansion using symmetry operators is just the special case of symmetry expansion in which our expansion operator $\Gamma_{\vec{w}}$ is the square of some other expansion operator: $\Gamma_{\vec{w}} = \Gamma_{\vec{v}}^\dagger \Gamma_{\vec{v}}$ such that $\rho_{\vec{w}}$ in Eq. (10) is guaranteed to be positive semi-definite and thus is a valid density operator.

To measure the effect of symmetry expansion and symmetry verification in mitigating the errors in the noisy observable $\langle O \rangle$, we can define the *fractional error in the*

observable estimate without and with symmetry expansion as:

$$\begin{aligned}\epsilon_0(O) &= \frac{\langle \psi_0 | O | \psi_0 \rangle - \text{Tr}(O\rho)}{\langle \psi_0 | O | \psi_0 \rangle} \\ \epsilon_{\vec{w}}(O) &= \frac{\langle \psi_0 | O | \psi_0 \rangle - \text{Tr}(O\rho_{\vec{w}})}{\langle \psi_0 | O | \psi_0 \rangle}.\end{aligned}\quad (13)$$

Ideally we would want to identify the symmetry expansion weights \vec{w} that minimised $|\epsilon_{\vec{w}}(O)|$. Since symmetry verification is simply a special case of symmetry expansion with $\vec{w} = \vec{1}$, by definition the optimised symmetry expansion should match or outperform symmetry verification:

$$|\epsilon_{\vec{1}}(O)| \geq \min_{\vec{w}} |\epsilon_{\vec{w}}(O)|.$$

Searching for the *exact* optimal symmetry expansion that minimise the absolute fractional errors is often impossible in practice. However, we will find a way to search for a symmetry expansion that can outperform symmetry verification.

III. SEARCHING FOR A GOOD SYMMETRY EXPANSION

A. Metric for a Good Symmetry Expansion

Using Eq. (13) with $O = \rho_0 = |\psi_0\rangle\langle\psi_0|$, which is just the ideal noiseless state, we then have:

$$|\epsilon_0(\rho_0)| = \epsilon_0(\rho_0) = 1 - \langle \psi_0 | \rho | \psi_0 \rangle = 1 - \langle \rho_0 \rangle \quad (14)$$

where $\langle \rho_0 \rangle$ is just the *fidelity* of the original noisy state against the ideal state $|\psi_0\rangle$, and thus $\epsilon_0(\rho_0)$ is simply the *infidelity* of the original noisy state.

Now using Eq. (10) and Eq. (11), we can obtain the symmetry-verified fidelity:

$$\langle \psi_0 | \rho_{\vec{1}} | \psi_0 \rangle = \frac{\langle \rho_0 \rangle}{\langle \Gamma_{\vec{1}} \rangle}, \quad (15)$$

which is just the original noisy fidelity boosted by a factor of $\langle \Gamma_{\vec{1}} \rangle^{-1}$. Hence, the infidelity of symmetry verification can be rewritten as:

$$|\epsilon_{\vec{1}}(\rho_0)| = \epsilon_{\vec{1}}(\rho_0) = 1 - \langle \psi_0 | \rho_{\vec{1}} | \psi_0 \rangle = 1 - \frac{\langle \rho_0 \rangle}{\langle \Gamma_{\vec{1}} \rangle}. \quad (16)$$

Just as the infidelities $|\epsilon_0(\rho_0)|$ or $|\epsilon_{\vec{1}}(\rho_0)|$ can be a metric in predicting the performance of using the noisy state ρ or the symmetry-verified state $\rho_{\vec{1}}$ instead of the ideal state ρ_0 for tasks like observable estimation, we would expect

$$|\epsilon_{\vec{w}}(\rho_0)| = |1 - \text{Tr}(\rho_0 \rho_{\vec{w}})| = |1 - \langle \psi_0 | \rho_{\vec{w}} | \psi_0 \rangle| \quad (17)$$

to also be a good metric in predicting the performance of using a general symmetry-expanded state $\rho_{\vec{w}}$. This will

be further verified in our numerical simulation later in Section V. We will call this the *absolute infidelity* of the symmetry expansion.

For the symmetry-expanded fidelity $\langle \psi_0 | \rho_{\vec{w}} | \psi_0 \rangle$, we can again use Eq. (10) and Eq. (11) to obtain:

$$\langle \psi_0 | \rho_{\vec{w}} | \psi_0 \rangle = \frac{\langle \rho_0 \rangle}{\langle \Gamma_{\vec{w}} \rangle} \quad (18)$$

which is just the original noisy fidelity $\langle \rho_0 \rangle$ boosted by a factor of $\langle \Gamma_{\vec{w}} \rangle^{-1}$. Note that even though we call $\langle \psi_0 | \rho_{\vec{w}} | \psi_0 \rangle$ symmetry-expanded fidelity, it is not bounded between 0 and 1 due to the fact that $\rho_{\vec{w}}$ is not necessarily positive semi-definite, thus it is not the fidelity in the usual sense. Eq. (17) can now be rewritten as:

$$|\epsilon_{\vec{w}}(\rho_0)| = \left| 1 - \frac{\langle \rho_0 \rangle}{\langle \Gamma_{\vec{w}} \rangle} \right|, \quad (19)$$

whose shape is plotted in Fig. 1.

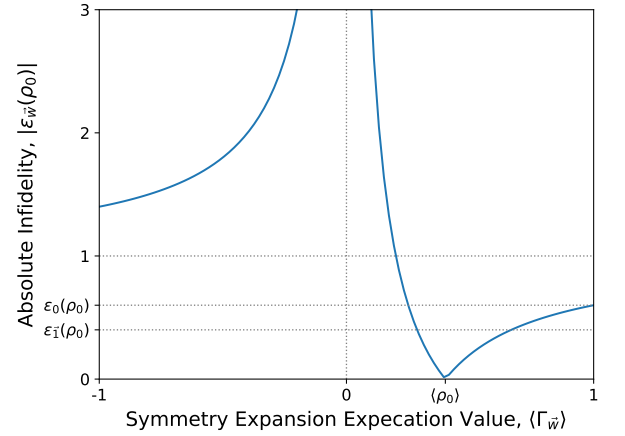


FIG. 1. This is a plot showing how the absolute infidelity of symmetry expansion with the weight distribution \vec{w} changes with the noisy expectation value of the symmetry expansion operator $\Gamma_{\vec{w}}$.

As we can see from Fig. 1, the expectation value of the expansion operator $\langle \Gamma_{\vec{w}} \rangle$ can lie within three different regions:

- $\langle \Gamma_{\vec{w}} \rangle \leq 0$:

This means that the majority of the state is driven out of the $\Gamma_{\vec{w}} = 1$ symmetry subspace. As seen from Fig. 1, we have $|\epsilon_{\vec{w}}(\rho_0)| \geq 1 \geq \epsilon_0(\rho_0)$, i.e. symmetry expansion will perform worse than the original noisy state. Hence, there is no point performing symmetry expansions in this region.

- $0 \leq \langle \Gamma_{\vec{w}} \rangle \leq \langle \rho_0 \rangle$:

Eq. (19) turns into:

$$|\epsilon_{\vec{w}}(\rho_0)| = -\epsilon_{\vec{w}}(\rho_0) = \frac{\langle \rho_0 \rangle}{\langle \Gamma_{\vec{w}} \rangle} - 1. \quad (20)$$

Using Eq. (14) and Eq. (16), the conditions for symmetry expansion to outperform the original noisy state and symmetry verification are

$$\begin{aligned} |\epsilon_{\bar{w}}(\rho_0)| \leq \epsilon_0(\rho_0) &\Rightarrow \langle \Gamma_{\bar{w}} \rangle^{-1} \leq 2 \langle \rho_0 \rangle^{-1} - 1, \\ |\epsilon_{\bar{w}}(\rho_0)| \leq \epsilon_{\bar{I}}(\rho_0) &\Rightarrow \langle \Gamma_{\bar{w}} \rangle^{-1} \leq 2 \langle \rho_0 \rangle^{-1} - \langle \Gamma_{\bar{I}} \rangle^{-1}. \end{aligned} \quad (21)$$

- $\langle \Gamma_{\bar{w}} \rangle \geq \langle \rho_0 \rangle$:

This is the only region that the symmetry-expanded fidelity $\langle \psi_0 | \rho_{\bar{w}} | \psi_0 \rangle$ behaves like the regular fidelity and is bounded between 0 and 1. Eq. (19) turns into:

$$|\epsilon_{\bar{w}}(\rho_0)| = \epsilon_{\bar{w}}(\rho_0) = 1 - \frac{\langle \rho_0 \rangle}{\langle \Gamma_{\bar{w}} \rangle}. \quad (22)$$

In this region, we always have $|\epsilon_{\bar{w}}(\rho_0)| \leq \epsilon_0(\rho_0)$, and thus symmetry expansion can always outperform the original noisy state. Using Eq. (16), the condition for symmetry expansion to outperform symmetry verification is

$$|\epsilon_{\bar{w}}(\rho_0)| \leq \epsilon_{\bar{I}}(\rho_0) \Rightarrow \langle \Gamma_{\bar{w}} \rangle \leq \langle \Gamma_{\bar{I}} \rangle.$$

In summary, symmetry expansion using the expansion operator $\Gamma_{\bar{w}}$ can outperform the original noisy state when

$$\langle \Gamma_{\bar{w}} \rangle^{-1} \leq 2 \langle \rho_0 \rangle^{-1} - 1, \quad (23)$$

and it can outperform symmetry verification when

$$\langle \Gamma_{\bar{I}} \rangle^{-1} \leq \langle \Gamma_{\bar{w}} \rangle^{-1} \leq 2 \langle \rho_0 \rangle^{-1} - \langle \Gamma_{\bar{I}} \rangle^{-1}. \quad (24)$$

The optimum can be reached at $\langle \Gamma_{\bar{w}} \rangle = \langle \rho_0 \rangle$ for which $|\epsilon_{\bar{w}}(\rho_0)| = 0$. Hence, to obtain the optimal symmetry expansion, we want to minimise $|\langle \Gamma_{\bar{w}} \rangle - \langle \rho_0 \rangle|$:

$$\min_{\bar{w}} |\langle \Gamma_{\bar{w}} \rangle - \langle \rho_0 \rangle| = \min_{\bar{w}} \left| \frac{\sum_{G \in \mathbb{G}} w_G (\langle G \rangle - \langle \rho_0 \rangle)}{\sum_{G \in \mathbb{G}} w_G} \right|. \quad (25)$$

To carry out this optimisation, we need to first estimate $\langle \rho_0 \rangle$ and $\langle G \rangle$. We can estimate $\langle \rho_0 \rangle$ using knowledge about the noise in the circuit as will be discussed in Section IV, and we can estimate $\langle G \rangle$ by directly sampling from the noisy circuit.

B. Near-Optimal Symmetry Expansions

Since in practice it is usually difficult to estimate $\langle \rho_0 \rangle$ to high accuracy, the minimisation in Eq. (25) often cannot be exactly carried out. A more practical way would be finding a scheme that minimise its upper bound:

$$\min_{\bar{w}} |\langle \Gamma_{\bar{w}} \rangle - \langle \rho_0 \rangle| \leq \min_{\bar{w}} \frac{\sum_{G \in \mathbb{G}} w_G |\langle G \rangle - \langle \rho_0 \rangle|}{\sum_{G \in \mathbb{G}} w_G}, \quad (26)$$

so that we can at least guarantee that it is near the optimum.

To do this, we will first try to find G_+ and G_- , which are the two symmetry operators that have their noisy expectation values $\langle G \rangle$ closest to $\langle \rho_0 \rangle$, one from above, one from below:

$$\begin{aligned} \langle G_+ \rangle - \langle \rho_0 \rangle &= \min_{\langle G \rangle \geq \langle \rho_0 \rangle} \langle G \rangle - \langle \rho_0 \rangle \\ \langle \rho_0 \rangle - \langle G_- \rangle &= \min_{\langle G \rangle < \langle \rho_0 \rangle} \langle \rho_0 \rangle - \langle G \rangle. \end{aligned} \quad (27)$$

The upper bound in Eq. (26) can now be rewritten as:

$$\begin{aligned} &\min_{\bar{w}} |\langle \Gamma_{\bar{w}} \rangle - \langle \rho_0 \rangle| \\ &\leq \min_{0 \leq w \leq 1} [w |\langle G_+ \rangle - \langle \rho_0 \rangle| + (1-w) |\langle G_- \rangle - \langle \rho_0 \rangle|]. \end{aligned}$$

Since $\langle G_+ \rangle - \langle \rho_0 \rangle$ is positive and $\langle G_- \rangle - \langle \rho_0 \rangle$ is negative, we can revert back to Eq. (25) and keeping only G_+ and G_- , so that they can cancel each other and give us a tighter upper-bound:

$$\min_{\bar{w}} |\langle \Gamma_{\bar{w}} \rangle - \langle \rho_0 \rangle| \leq \min_{0 \leq w \leq 1} |w \langle G_+ \rangle + (1-w) \langle G_- \rangle - \langle \rho_0 \rangle|. \quad (28)$$

Therefore, our *near-optimal* symmetry expansion will only contain the two symmetries: G_+ and G_- , with their weights being w and $1-w$, respectively. As mentioned, in practice it may be hard to estimate $\langle \rho_0 \rangle$ to high enough accuracy to exactly carry out the above optimisation. Hence, we will instead look at two different scenarios and construct the near-optimal symmetry expansions for them separately.

- *Biased-weight scheme:*

Suppose we have $\langle G_+ \rangle$ much closer to $\langle \rho_0 \rangle$ than $\langle G_- \rangle$, or maybe we have all $\langle G \rangle \geq \langle \rho_0 \rangle$ such that there is no G_- , in these cases we will set $w = 1$ in Eq. (28), which means our symmetry expansion consist of only one symmetry operator G_+ . Similarly if the opposite happens, we will turn to the $w = 0$ scheme, which means our symmetry expansion consists of only G_- . For these two expansion schemes, we have:

$$\langle \Gamma_{G_{\pm}} \rangle = \langle G_{\pm} \rangle. \quad (29)$$

- *Equal-weight scheme:*

For all the other non-extreme cases, the most practical scheme is to have equal weights for G_+ and G_- , which is just $w = 1/2$ in Eq. (28). We will denote the weight distribution as \vec{w}_{\pm} and we have:

$$\langle \Gamma_{\vec{w}_{\pm}} \rangle = \frac{1}{2} (\langle G_+ \rangle + \langle G_- \rangle). \quad (30)$$

C. Equivalent Symmetry

If a given symmetry operator S commutes with the noisy state ρ , which also implies S^{-1} commuting with ρ , we then have:

$$\langle G \rangle = \text{Tr}(S^{-1} S G \rho) = \text{Tr}(S G S^{-1} \rho) = \langle S G S^{-1} \rangle. \quad (31)$$

One possible way that such a symmetry S can arise is when it corresponds to some qubit permutations. In such a case, we would naturally design a state preparation circuit with a layout that respects this symmetry. Since we usually assume the nature of the noise of a given type of circuit components is the same for all of its instances in the circuit, we can expect the resultant noisy state ρ coming out of this circuit will also follow the same symmetry: $S\rho S^{-1} = \rho$, i.e. ρ commutes with S .

Using Eq. (9), the symmetry expansion expected value can be written as:

$$\langle \Gamma_{\vec{w}} \rangle = \frac{\sum_{G \in \mathbb{G}} w_G \langle G \rangle}{\sum_{G \in \mathbb{G}} w_G}. \quad (32)$$

Eq. (31) implies we can obtain the same value for $\langle \Gamma_{\vec{w}} \rangle$ even if we sample SGS^{-1} in place of G . Hence, G and SGS^{-1} are equivalent when we are considering $\langle \Gamma_{\vec{w}} \rangle$, which in turn means they are equivalent when we want to minimise the absolute infidelity $|\epsilon_{\vec{w}}(\rho_0)|$ using Eq. (25).

We will denote the set of symmetry operators that commute with ρ as \mathbb{S} , which is a subgroup of \mathbb{G} . We say that two elements G and G' are equivalent if they give the same noisy expectation value. Alternatively, based on our arguments above, we can write this as

$$G \sim G' \quad \text{iff } \exists S \in \mathbb{S} \quad SGS^{-1} = G'.$$

We can prove that this is an equivalence relation, and thus will partition the whole symmetry group into different equivalent classes. The symmetry operator within each equivalent class will have the same effect when sampled in symmetry expansion for calculating the fidelity against the ideal states. Hence, to find the optimal symmetry expansion, we only need to pick *one element from each equivalent class* and sample over them instead of sampling over the whole symmetry group. This vastly reduces the search space for the optimal sampling distribution. In the extreme case that ρ commutes with all symmetry operators $G \in \mathbb{G}$, then the equivalent classes are just the conjugacy classes of \mathbb{G} .

D. Intuition behind Good Symmetry Expansion

Now we will try to understand why symmetry expansion may offer better performance than symmetry verification through the simple example in which there is just one single non-trivial symmetry operator: $\mathbb{G} = \{I, G\}$.

We will use P_u/P_d to denote the probability that some errors undetectable/detectable by the symmetry G have occurred in a given circuit run. Recall that $\langle \rho_0 \rangle$ is the fidelity of the noisy state against the ideal state and $\langle \Gamma_{\vec{1}} \rangle$ is the probability of passing the symmetry verification, we have:

$$\begin{aligned} \langle \rho_0 \rangle &\sim 1 - P_u - P_d \\ \langle \Gamma_{\vec{1}} \rangle &\sim 1 - P_d \\ \langle G \rangle &= 2 \langle \Gamma_{\vec{1}} \rangle - 1 \sim 1 - 2P_d. \end{aligned}$$

Hence, using Eq. (14), Eq. (16) and Eq. (19), the absolute infidelities of various schemes are:

$$\begin{aligned} \epsilon_0(\rho_0) &\sim P_u + P_d \\ \epsilon_{\vec{1}}(\rho_0) &\sim \frac{P_u}{1 - P_d} \\ |\epsilon_{\vec{w}}(\rho_0)| &\sim \left| \frac{P_u - P_d}{1 - 2P_d} \right|. \end{aligned} \quad (33)$$

We see that $\epsilon_0(\rho_0)$ is proportional to the *sum* of P_u and P_d since none of the errors are removed, $\epsilon_{\vec{1}}(\rho_0)$ is proportional to just P_u since only the detectable errors are removed by symmetry verification. On the other hand, $|\epsilon_{\vec{w}}(\rho_0)|$ is proportional to the *difference* between P_u and P_d , allowing *cancellation* between detectable and undetectable error probability, which is why it might be more effective than symmetry verification.

IV. PAULI SYMMETRY

A. Implementation

To perform symmetry verification for a general symmetry group, we can have an ancilla register with its different basis states corresponding to different elements in the group, then perform control-symmetry operations from the ancilla to the data register and measure out the ancilla as outlined in Ref. [14]. For Pauli symmetry groups (stabiliser groups), their symmetry verification can be carried out by simply measuring the group *generators* since they are abelian, and thus is much more relevant to practical implementations and will be our focus in this section.

In direct symmetry verification, we need to measure the whole set of symmetry generators and the observable in the same circuit run, and discard runs that fail *any* of the symmetry tests. This can be difficult in practice since we usually can only implement local measurements while these symmetry generators and the observable might not locally commute with each other. The problem could become worse in practice since we usually need to measure multiple observables in the same circuit run to save the sampling cost. To solve this, we will need to use additional circuit structures to simultaneously diagonalise all the observables and symmetries we want to measure [17, 18]. We can vastly alleviate this problem by using post-processing symmetry verification and more generally symmetry expansion, within which we only need to measure one symmetry operator along with the observables in each circuit run.

Since we are discarding circuit runs that fail the symmetry test in direct symmetry verification, we are essentially changing the form of the effective error channels in the circuit. Therefore combining direct symmetry verification with other error mitigation techniques like quasi-probability and error extrapolation would require elaborate schemes [5] since they all rely on our knowledge

about the error channels. On the other hand, there is no discarding circuit runs in symmetry expansion, and thus it can be combined with other error mitigation techniques more straightforwardly.

B. Sampling Cost

Now looking beyond the circuit implementation, we would want to know how many circuit runs are needed for different error mitigation schemes. Suppose we need CN circuit runs to reach a given precision for an observable with quantum error mitigation and N circuit runs without, then C is defined to be the *sampling cost* for the given quantum error mitigation method. As shown in Appendix B, the sampling cost for implementing *direct* symmetry verification and symmetry expansion are

$$C_{dir} \sim \langle \Gamma_{\vec{1}} \rangle^{-1}, \quad C_{\vec{w}} \sim \langle \Gamma_{\vec{w}} \rangle^{-2}. \quad (34)$$

As discussed in Section III A, in the region where $\langle \Gamma_{\vec{w}} \rangle \geq \langle \rho_0 \rangle$, the symmetry-expanded fidelity behaves like regular fidelity and thus can be used as a performance metric for symmetry expansion. For all symmetry expansions in this region, including post-processing symmetry verification, if we are allowed C sampling cost for our error mitigation technique, symmetry expansion can give us a factor of \sqrt{C} boost in the fidelity based on Eq. (18) and Eq. (34). Hence, we see that symmetry expansion in this regime is as ‘cost-effective’ as post-processing symmetry verification. Direct symmetry verification, on the other hand, can achieve a factor of C boost in the fidelity and thus is more ‘cost-effective’ but is more difficult to implement due to the measurement requirement and harder to combine with other error mitigation techniques as discussed in Section IV A.

In the region where $\langle \Gamma_{\vec{w}} \rangle < \langle \rho_0 \rangle$, the symmetry-expanded fidelity is not well-defined anymore and thus our performance metric becomes the absolute infidelity as discussed in Section III A. In this region we can achieve the same performance as the symmetry expansion in the $\langle \Gamma_{\vec{w}} \rangle \geq \langle \rho_0 \rangle$ region, but at a smaller $\langle \Gamma_{\vec{w}} \rangle$ and thus at a larger sampling cost $C_{\vec{w}}$. Hence, symmetry expansion in this region is less ‘cost effective’ than post-processing symmetry verification.

C. Estimation of Fidelity and Symmetry Observables

To compare between symmetry expansion and symmetry verification, we need to first estimate $\langle \rho_0 \rangle$ and $\langle \Gamma_{\vec{w}} \rangle$.

We will call the expected number of errors occurring in each circuit run the *mean circuit error count* and denote it using μ . In practical NISQ application, we would expect to have a circuit that is large enough such that the number of error locations is much greater than 1 and is not too noisy such that the mean circuit error count is of

order unity: $\mu \sim 1$. In this limit, using the Le Cam’s theorem, the probability that n errors occurring in a given circuit run will follow the Poisson distribution provided the noise is Markovian:

$$P_n = e^{-\mu} \frac{\mu^n}{n!}.$$

Hence, the probability that there is no errors in the circuit will be:

$$P_0 = e^{-\mu}.$$

Suppose the fraction of errors that result in erroneous states orthogonal to the ideal state $|\psi_0\rangle$ is f_ϵ , while we will assume the rest of the errors act trivially on $|\psi_0\rangle$. Then the effective error rate we have is $f_\epsilon \mu$, and the fidelity $\langle \rho_0 \rangle$ is just the probability that zero effective errors happens:

$$\langle \rho_0 \rangle \sim P_0 = e^{-f_\epsilon \mu}. \quad (35)$$

For a given Pauli symmetry G , if we can approximately decomposed all noise channels within each error location into components that are detectable by G and components that are undetectable, with f_G being the fraction of errors detectable by G averaged over all error locations, then as shown in Appendix A, we have:

$$\langle G \rangle \sim e^{-2f_G \mu}. \quad (36)$$

Using Eq. (9), we then have:

$$\langle \Gamma_{\vec{w}} \rangle = \frac{\sum_{G \in \mathbb{G}} w_G \langle G \rangle}{\sum_{G \in \mathbb{G}} w_G} \sim \frac{\sum_{G \in \mathbb{G}} w_G e^{-2f_G \mu}}{\sum_{G \in \mathbb{G}} w_G} \quad (37)$$

Note that $f_I = 0$.

D. Near-Optimal Pauli Symmetry Expansions

Here we will try to apply the arguments in Section III B to Pauli symmetry. Using Eq. (35) and Eq. (36), we can rewrite Eq. (27) as

$$G_+ = \arg \min_{G \in \mathbb{G}, 2f_G \geq f_\epsilon} f_G, \quad G_- = \arg \max_{G \in \mathbb{G}, 2f_G < f_\epsilon} f_G,$$

i.e. G_+ and G_- are the two symmetry operators that has their fraction of detectable errors f_G closest to $f_\epsilon/2$, one from above, one from below. In the case we cannot estimate f_ϵ accurately, we can make the simple assumption that all errors will lead to orthogonal erroneous states and thus $f_\epsilon = 1$. This in turn means that G_+ and G_- are the two symmetry operators that have their fraction of detectable errors f_G closest to $1/2$. Of course, when we cannot estimate f_G accurately, we can always fall back onto Eq. (27).

In the context of Pauli symmetry, we can further analyse the performance and cost of near-optimal schemes in Section III B.

Biased-weight scheme

Using Eq. (29) and Eq. (36), we can write the biased-weight expansion operator as

$$\langle \Gamma_{G_{\pm}} \rangle = \langle G_{\pm} \rangle = e^{-2f_{G_{\pm}}\mu}.$$

Hence, using Eq. (19) and Eq. (35), we can obtain the absolute infidelity:

$$|\epsilon_{G_{\pm}}(\rho_0)| = \left| 1 - e^{(2f_{G_{\pm}} - f_{\epsilon})\mu} \right|. \quad (38)$$

Using Eq. (34), the sampling cost for the near-optimal symmetry expansion is

$$C_{G_{\pm}} = \langle \Gamma_{G_{\pm}} \rangle^{-2} = e^{4f_{G_{\pm}}\mu}. \quad (39)$$

Since $f_{G_{\pm}}$ and $f_{\epsilon}/2$ are by definition very close, we should have small $|2f_{G_{\pm}} - f_{\epsilon}|\mu$. The absolute infidelity and cost of the near-optimal scheme can then be simplified to:

$$\begin{aligned} |\epsilon_{G_{\pm}}(\rho_0)| &\approx |2f_{G_{\pm}} - f_{\epsilon}|\mu \\ C_{G_{\pm}} &\approx e^{4f_{G_{\pm}}\mu} \sim e^{2f_{\epsilon}\mu} \sim e^{2\mu}. \end{aligned} \quad (40)$$

Equal-weight scheme

Now using Eq. (30) and Eq. (36), we can write the equal-weight expansion operator as

$$\begin{aligned} \langle \Gamma_{\bar{w}_{\pm}} \rangle &= \frac{1}{2} \left(e^{-2f_{G_-}\mu} + e^{-2f_{G_+}\mu} \right) \\ &= e^{-(f_{G_+} + f_{G_-})\mu} \cosh((f_{G_+} - f_{G_-})\mu). \end{aligned}$$

Using Eq. (19), the absolute infidelity is:

$$|\epsilon_{\bar{w}_{\pm}}(\rho_0)| = \left| 1 - \frac{e^{-(f_{G_+} + f_{G_-} - f_{\epsilon})\mu}}{\cosh((f_{G_+} - f_{G_-})\mu)} \right|. \quad (41)$$

Using Eq. (34), the sampling cost for the near-optimal symmetry expansion is

$$C_{\bar{w}_{\pm}} = \langle \Gamma_{\bar{w}_{\pm}} \rangle^{-2} = \frac{e^{2(f_{G_+} + f_{G_-})\mu}}{\cosh^2((f_{G_+} - f_{G_-})\mu)}. \quad (42)$$

Since f_{G_-} and f_{G_+} are by definition both very close to $f_{\epsilon}/2$, we should have small $(f_{G_+} - f_{G_-})\mu$ and small $(f_{G_+} + f_{G_-} - f_{\epsilon})\mu$. The absolute infidelity and cost of the near-optimal scheme in Eq. (41) and Eq. (42) can then be simplified to:

$$\begin{aligned} |\epsilon_{\bar{w}_{\pm}}(\rho_0)| &\approx |f_{G_+} + f_{G_-} - f_{\epsilon}|\mu \\ C_{\bar{w}_{\pm}} &\approx e^{2(f_{G_+} + f_{G_-})\mu} \sim e^{2f_{\epsilon}\mu} \sim e^{2\mu}. \end{aligned} \quad (43)$$

Looking at Eq. (40) and Eq. (43), we see that in both near-optimal schemes the absolute infidelity grow with the mean circuit error count μ linearly at the slow rate of

$|f_{G_+} + f_{G_-} - f_{\epsilon}|$ and $|2f_{G_{\pm}} - f_{\epsilon}|$. The sampling cost on the other hand grow exponentially with the mean circuit error count μ , similar to other mainstream quantum error mitigation techniques [6].

Beyond Pauli symmetry, an example for symmetry expansion is the virtual distillation scheme mentioned in Section I. The way it relates to symmetry expansion is outlined in Appendix C. Being a symmetry expansion scheme, it was shown to be outperforming the corresponding symmetry verification scheme via both theoretical analysis and numerical simulations [11, 12]. In the next section, we will continue to focus on Pauli symmetry and look into a numerical simulation example with inherent Pauli symmetry.

V. NUMERICAL SIMULATION

A. Problem Setup

The physical problem that we will be looking at is the 2D Fermi-Hubbard model with nearest-neighbour interaction, with the Hamiltonian given as:

$$H = - \underbrace{\sum_{\sigma, \langle v, w \rangle} t_{v, w} (a_{v, \sigma}^{\dagger} a_{w, \sigma} + a_{w, \sigma}^{\dagger} a_{v, \sigma})}_{\text{nearest-neighbour hopping}} + \underbrace{\sum_v U_v n_{v, \uparrow} n_{v, \downarrow}}_{\text{onsite repulsion}}. \quad (44)$$

Here $a_{v, \sigma}^{\dagger}/a_{v, \sigma}$ are the creation/annihilation operators of site v with spin σ and $n_{v, \uparrow/\downarrow}$ are the number operators. The exact circuit we used is outlined in Ref. [19], which has the same form as a first-order trotterisation circuit. We use the Jordan-Wigner encoding to map the individual interaction terms and fermionic swaps to two-qubit gates in the circuit, with the gates that correspond to the interaction terms parametrised. This circuit can be used in for example variational eigen-solvers. All two-qubit gates are assumed to be affected by two-qubit *depolarising noise* of the same strength.

We will look at a range of circuits with randomly generated parameters and thus has random ideal output states. Using $t_{v, w} = 1$ and $U_v = 2$ for our Hamiltonian, we can measure the energy of the ideal output state and compare it to the energies of the noisy output state and the error-mitigated output states. In our simulation, we will focus on circuits whose ideal output energies *magnitude* are larger than 0.5 since in practice we are usually interested in states with non-negligible energy magnitude (otherwise the sampling cost for high energy precision will be very large).

B. Finding Near-Optimal Symmetry Expansion

The ideal circuit will conserve the number of fermions within each spin subspace. Hence, the symmetry operator we can enforce on the output state would be

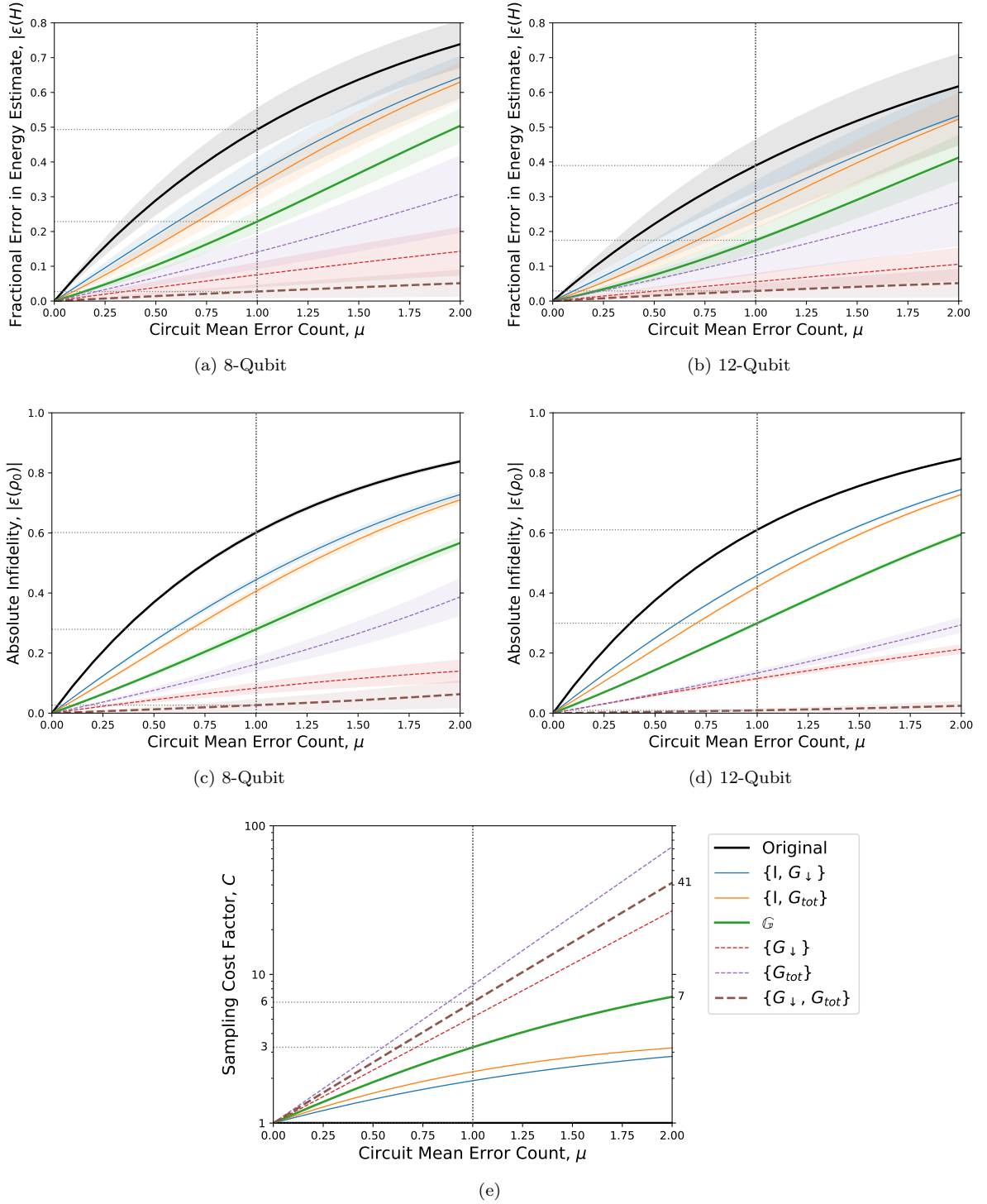


FIG. 2. Performance metrics for different symmetry expansion schemes against the increase of mean circuit error count: the magnitude of the fractional error in the energy estimate for (a) 8-qubit and (b) 12-qubit simulations; the magnitude of infidelity for (c) 8-qubit and (d) 12-qubit simulations; (e) the sampling cost for all simulations. Data are averaged over circuit configurations with randomly generated parameters with the shaded areas indicating the spread of the lines over different parameters. The 8-qubit simulation corresponds to 2×2 half-filled Fermi-Hubbard model and has 144 two-qubit gates. The 12-qubit simulation corresponds to 2×3 half-filled Fermi-Hubbard model and has 336 two-qubit gates. The legend indicates the set of symmetry operators used in the corresponding symmetry expansion, all with uniform weight distribution. All the symmetry verifications are labelled using solid lines, while all other symmetry expansion are labelled using dashed lines. Three of the most representative methods: the original noisy state, the symmetry verification using the full symmetry group \mathbb{G} and the near-optimal symmetry expansion using $\{G_{\downarrow}, G_{tot}\}$ with equal weight are labelled with thickened lines. Note that since G_{\uparrow} and G_{\downarrow} are almost equivalent for the purpose of symmetry expansion, we have only shown expansions for G_{\downarrow} here for visual clarity.

the spin-up/down number parity symmetry, denoted as $G_{\uparrow/\downarrow}$. In the Jordan-Wigner encoding, $G_{\uparrow/\downarrow}$ is just the tensor product of the Z operators acting on the qubits corresponding to the spin-up/down orbitals. Together they can generate the number parity symmetry group $\mathbb{G} = \{I, G_{\uparrow}, G_{\downarrow}, G_{tot}\}$, where $G_{tot} = G_{\uparrow}G_{\downarrow}$ is the total fermion number parity symmetry.

The Hamiltonian in Eq. (44) is invariant under exchange of spin up and spin down. This spin-exchange symmetry is denoted as S , and will naturally lead to a circuit construction that respects S . Hence, as shown in Section III C, we can prove that G_{\uparrow} and the corresponding conjugated symmetry $SG_{\uparrow}S^{-1} = G_{\downarrow}$ would be equivalent when used for symmetry expansion. However, for our practical implementation of the circuit, the trotter step implemented actually does not *exactly* commute with S . Therefore, the performance of G_{\uparrow} and G_{\downarrow} for symmetry expansion are only *approximately* the same in our case. However, they are close enough such that we will only consider G_{\downarrow} when we look over different symmetry expansion schemes in our simulation to simplify our comparison between different expansions.

As shown in Appendix D, the fraction of errors detectable by G_{tot} is estimated to be $f_{G_{tot}} \sim \frac{8}{15}$ and that by $G_{\uparrow/\downarrow}$ is estimated to be $f_{G_{\uparrow/\downarrow}} \sim \frac{2}{5}$. If we assume the fraction of errors that will lead to an erroneous state orthogonal to the ideal state is $f_e = 1$, we then have both $f_{G_{tot}}$ and $f_{G_{\uparrow/\downarrow}}$ are very close to $f_e/2$, one larger and one smaller. Hence, following the discussion in Section III B, we have:

$$G_+ = G_{tot}, \quad G_- = G_{\uparrow/\downarrow}.$$

The near-optimal symmetry expansion in this case will be the equal-weight expansion using $G_{\uparrow/\downarrow}$ and G_{tot} , with the expansion operator being

$$\Gamma_{\vec{w}\pm} = \frac{1}{2} (G_{\uparrow/\downarrow} + G_{tot}). \quad (45)$$

C. Results

The absolute fractional error in the energy estimate, denoted as $|\epsilon(H)|$ over different mean circuit error counts μ for the 8-qubit and 12-qubit simulations are shown in Fig. 2 (a) and (b). The corresponding absolute infidelity $|\epsilon(\rho_0)|$ are shown in Fig. 2 (c) and (d). From the close resemblance between the shapes of the curves for $|\epsilon(H)|$ and $|\epsilon(\rho_0)|$, we see that $|\epsilon(\rho_0)|$ is indeed a good performance metric for comparing different symmetry expansion methods and predicting the change of performance over different μ . This further validates our approach of searching for good symmetry expansions based on $|\epsilon(\rho_0)|$ in Section III and Section IV.

Here we will only compare among symmetry expansions with *uniform weights* but with *different sets of symmetry operators*. We see that in our examples in Fig. 2, the symmetry expansions that correspond to symmetry verifications (solid lines) are outperformed by the

other symmetry expansions (dashed lines), with the near-optimal scheme we found in Section V B achieving the lowest fractional errors and thus the best performance.

The sampling costs are shown in Fig. 2 (e), which is essentially the plot of the function $C_{\vec{w}} = \langle \Gamma_{\vec{w}} \rangle^{-2}$ in Eq. (34) for different \vec{w} . Since the estimated detectable error fraction $f_{G_{\uparrow/\downarrow}}$ and $f_{G_{tot}}$ are independent of the number of qubits and the circuit parameters, it means that $\langle \Gamma_{\vec{w}} \rangle$ is mostly independent of the number of qubits and the circuit parameters using Eq. (37), and thus our cost plot is practically the same for both the 8-qubit and 12-qubit cases and for circuits with any parameters. Note that the cost for the symmetry verifications here are for post-processing verification. If we go for direct verification instead, then we need to take the square root of the cost.

	8-Qubit		12-Qubit		Cost
	$ \epsilon(H) $	$ \epsilon(\rho_0) $	$ \epsilon(H) $	$ \epsilon(\rho_0) $	
Original	0.493	0.601	0.390	0.610	1.0
Verified	0.229	0.279	0.175	0.299	3.2
Expanded	0.027	0.027	0.029	0.009	6.5

(a) $\mu = 1$

	8-Qubit		12-Qubit		Cost
	$ \epsilon(H) $	$ \epsilon(\rho_0) $	$ \epsilon(H) $	$ \epsilon(\rho_0) $	
Original	0.739	0.838	0.618	0.848	1.0
Verified	0.504	0.567	0.413	0.595	7.1
Expanded	0.051	0.063	0.051	0.025	41.4

(b) $\mu = 2$

TABLE I. The fractional error in energy estimate $|\epsilon(H)|$, absolute infidelity $|\epsilon(\rho_0)|$, and the sampling costs for three of the most representative symmetry expansions in our simulation: the original noisy state (Original), the symmetry verification using the full symmetry group \mathbb{G} (Verified) and the near-optimal symmetry expansion using $\{G_{\downarrow}, G_{tot}\}$ with equal weight (Expanded) at the mean circuit error rate (a) $\mu = 1$ and (b) $\mu = 2$. Note that the cost for symmetry verification here are for post-processing symmetry verification.

Let us zoom in at the mean circuit error count $\mu = 1$ and focusing on the three most representative symmetry expansions (thicken lines): the original noisy state, the symmetry verification using the full symmetry group \mathbb{G} and the near-optimal symmetry expansion using $\{G_{\downarrow}, G_{tot}\}$ with equal weight, whose data are summarised in Table I (a). We see that at $\mu = 1$, the fractional energy estimate error $|\epsilon(H)|$ for the original noisy output sits at ~ 0.5 for the 8-qubit example and ~ 0.4 for the 12-qubit example. Symmetry verification using \mathbb{G} can reduce this fractional energy error to ~ 0.2 , more than halving the fractional errors, at the sampling cost of ~ 3 . This fractional error in the energy estimate can be further reduced to ~ 0.03 when we apply the near-optimal

expansion scheme in Eq. (45), which is ~ 15 times reduction compared to the original noisy state and ~ 6 times reduction compared to the symmetry verification. The sampling cost for the symmetry expansion is ~ 6 , which is only twice of the cost of the (post-process) symmetry verification. We see similar, if not larger, improvement of the absolute infidelity $|\epsilon(\rho_0)|$ by using the near-optimal symmetry expansion scheme over the original noisy state and symmetry verification.

Now we will move to $\mu = 2$ with the data summarised in Table I (b). The fractional energy estimate error $|\epsilon(H)|$ for the original noisy output now rise to ~ 0.74 for the 8-qubit example and ~ 0.62 for the 12-qubit example. Symmetry verification can reduce the fractional error to ~ 0.5 and ~ 0.4 for the 8-qubit and 12-qubit case, respectively, with a sampling cost of ~ 7 . Near-optimal symmetry expansion on the other hand can still achieve a low fractional error of ~ 0.05 , which is around 13 times reduction compared to the original state and around 9 times reduction compared to symmetry verification. However, due to the high circuit error rate $\mu = 2$, the near-optimal symmetry expansion would have a high sampling cost of ~ 41 . Such a sampling cost might be impractical in certain situations, in which we might want to turn to other symmetry expansion schemes like the biased-weight symmetry expansion with only the G_\downarrow operator in the expansion. As seen from Fig. 2, this biased-weight (single-operator) scheme can still achieve a lower energy estimate fractional error than symmetry verification at $|\epsilon(H)| \sim 0.14$ and at a more manageable sampling cost at ~ 27 . Similar to the $\mu = 1$ case, again we see similar if not larger improvements in the absolute infidelity $|\epsilon(\rho_0)|$ compared to $|\epsilon(H)|$ when we use the near-optimal symmetry expansion.

VI. CONCLUSION

In this article, we have constructed a general framework named *symmetry expansion* for symmetry-based error mitigation techniques. Different symmetry expansions correspond to different sampling weight distributions among the symmetry operators, with symmetry verification corresponding to the uniform weight distribution. Since symmetry verification is just a special case under the symmetry expansion framework, if we can find the optimal symmetry expansion weight for the estimation of a noisy observable, we should expect this optimal scheme to outperform symmetry verification. The effective ‘density operator’ after symmetry expansion is not positive semi-definite, thus instead of using the fidelity against the ideal state to predict the performance of a given symmetry expansion, we introduced the metric *absolute infidelity* against the ideal state to predict its performance, which essentially measures the distance of the symmetry-expanded ‘fidelity’ from 1. Using the absolute infidelity as the performance metric, we have introduced ways to search for a *near-optimal* symmetry expansion

weight. In the case of Pauli symmetry, we have shown ways to predict the performance and sampling cost of a given symmetry expansion scheme using our knowledge about the error channels in the circuit.

We then applied our methods to the energy estimation of Fermi-Hubbard model simulation with random circuit parameters for both the 8-qubit and 12-qubit cases. From our simulation, we see that indeed absolute infidelity is a good metric for predicting the *fractional* error in our energy estimate. When there is on average 1 error per circuit run, the fractional energy estimation errors can be reduced from $0.4 \sim 0.5$ for the original noisy state and ~ 0.2 for symmetry verification to ~ 0.03 for the near-optimal symmetry expansion. The sampling cost for symmetry verification in this case is 3, i.e. we need 3 times more circuit runs for shot noise reduction, while the sampling cost for the near-optimal symmetry expansion is around 6. Hence, symmetry expansion can reach an estimation accuracy 6 times beyond what is achievable by symmetry verification, and the sampling cost for shot noise reduction is only 2 times higher. When there is on average 2 errors per circuit run, we found that the amount of error reduction brought by the near-optimal symmetry expansion further increases, but the sampling cost also rise to 41 due to the high circuit error rate. In such a case, we might want to turn to other symmetry expansion schemes. In general, symmetry expansion provides us with a wider range of symmetry-based schemes beyond symmetry verification to fit our requirements on the balance between estimation errors and sampling costs.

The estimation errors of the symmetry expansion can be further improved if we could develop effective schemes to search for a more optimal symmetry expansion, which could be done by for example constructing a better performance metric beyond the absolute infidelity or using Clifford approximation learning-based method outlined in Ref. [20].

In this article, we have only considered positive sampling weights for symmetry expansion and it would be natural to extend this to negative sampling weights like in the quasi-probability error mitigation [3, 4]. On the other hand, it would also be interesting to see if any method can be developed to modify the sampling distribution within quasi-probability like how we go from symmetry verification to symmetry expansion. Part of this has been explored in Ref. [20].

We have provided an explicit example of the application of symmetry expansion for Pauli symmetry group (Section IV) and for virtual distillation (Appendix C) in this article. One could look into the more detailed application of symmetry expansion in the other cases, especially for non-abelian symmetry group since non-abelian symmetry expansion is much easier to implement than direct non-abelian symmetry verification, as non-abelian symmetry verification cannot be done by simply measuring their generators. However in this case, the expectation values of the symmetry operators might not be real

any more, and thus we need to redevelop our methods for finding a suitable symmetry expansion, possibly involving using complex weights. We might use methods in Ref. [21] to measure such complex expectation values.

All of our symmetry expansion arguments are directly applicable to the stabiliser symmetry group in the stabiliser codes. It would be interesting to look at an explicit example of how symmetry expansion might perform in the context of stabiliser code like what has been done for quantum subspace expansion [10]. To find the optimal symmetry expansion in this context, one might want to draw inspiration from Ref. [22] about ways to reduce the search space.

ACKNOWLEDGEMENTS

The numerical simulations are performed using QuESTlink [23], which is the Mathematica interface of the high-performance quantum computation simulation package QuEST [24]. The author is grateful to those who have contributed to both these valuable tools.

The author would like to thank Simon Benjamin and Balint Koczor for valuable discussions and Tyson Jones for his help on the usage of QuESTlink.

The author is supported by the Junior Research Fellowship from St John's College, Oxford and acknowledges support from the QCS Hub (EP/T001062/1).

Appendix A: Estimation of symmetry expectation values

Arguments in this section largely follows from Ref. [5]. We will assume the average number of errors in each circuit run is μ . Now looking within each error location in the circuit, there will be only a fraction of the errors can be detected by a given symmetry G . We will denote this detectable error fraction *averaged over all error locations* as f_G . Correspondingly, it means that the average number of such detectable errors in each circuit run will be $f_G\mu$. If the number of error locations with non-negligible detectable error components is much larger than 1, then following the same arguments in Eq. (18) while focusing on only detectable errors, the probability that n *detectable* errors occur in a given circuit run is:

$$P_n = e^{-f_G\mu} \frac{(f_G\mu)^n}{n!}.$$

For a Pauli symmetry G , only an odd number of such detectable errors will be detected and an even number of such detectable errors will pass the symmetry test. Hence, using Π_G to denote the projector into the $G = +1$ subspace, the probability of passing the symmetry test using G is just:

$$\langle \Pi_G \rangle = \sum_{\text{even } n} P_n = e^{-f_G\mu} \cosh(f_G\mu) = \frac{1 + e^{-2f_G\mu}}{2}.$$

Hence, we have:

$$\langle G \rangle = 2 \langle \Pi_G \rangle - 1 = e^{-2f_G\mu}.$$

Hence, the more general projection operator with multiple Pauli symmetries is simply:

$$\langle \Pi_{\mathbb{G}} \rangle \approx \frac{1}{|\mathbb{G}|} \sum_{G \in \mathbb{G}} e^{-2f_G\mu}. \quad (\text{A1})$$

where f_G is the fraction of errors that are detectable by G . Note that $f_I = 0$.

Now we look at a group of Pauli symmetry \mathbb{G} generated by the generators \tilde{G} . If the errors detectable by different symmetry generators $\tilde{G} \in \tilde{\mathbb{G}}$ are independent, i.e. each error component is *detectable and only detectable* by one of the symmetry generators $\tilde{G} \in \tilde{\mathbb{G}}$, then the symmetry tests using different symmetry generators will be independent. Hence, we have:

$$\langle \Pi_{\mathbb{G}} \rangle \approx \prod_{\tilde{G} \in \tilde{\mathbb{G}}} \langle \Pi_{\tilde{G}} \rangle = \prod_{\tilde{G} \in \tilde{\mathbb{G}}} \frac{1 + e^{-2f_{\tilde{G}}\mu}}{2}.$$

which is a special case of Eq. (A1).

Appendix B: Sampling Cost Analysis

In this section, we will follow the discussion in Section II, in which our circuit outputs the noisy quantum state ρ and we want to estimate the value of an observable O by using the symmetry verification with the symmetry projection operator $\Pi_{\mathbb{G}}$ or using symmetry expansion with the expansion operator $\Gamma_{\vec{w}}$. For simplicity, we will only consider Pauli symmetries and Pauli observables.

If we have a variable C that is obtained by taking the quotient of two other variables A and B :

$$C = \frac{A}{B},$$

then the variance of C can be approximated using:

$$\text{Var}[C] = \frac{1}{\langle B \rangle^2} \left[\text{Var}[A] - 2 \langle C \rangle \text{Cov}[A, B] + \langle C \rangle^2 \text{Var}[B] \right]. \quad (\text{B1})$$

Throughout this section, we will use \overline{X} to denote the estimator of $\langle X \rangle$ after N *circuit runs*. If in each circuit run, we can obtain one sample of A and one sample of B , then by definition, we have:

$$\overline{C} = \frac{\overline{A}}{\overline{B}}$$

and

$$\begin{aligned} \text{Var}[\overline{C}] &= \frac{1}{\langle B \rangle^2} \left[\text{Var}[\overline{A}] - 2 \langle C \rangle \text{Cov}[\overline{A}, \overline{B}] + \langle C \rangle^2 \text{Var}[\overline{B}] \right] \\ &= \frac{1}{N \langle B \rangle^2} \left[\text{Var}[A] - 2 \langle C \rangle \text{Cov}[A, B] + \langle C \rangle^2 \text{Var}[B] \right]. \end{aligned} \quad (\text{B2})$$

1. Direct Symmetry Verification

The symmetry-verified expectation value is:

$$\langle O_{dir} \rangle = \text{Tr}(O\rho_{sym}) = \frac{\text{Tr}(O\Pi_G\rho\Pi_G)}{\text{Tr}(\Pi_G\rho)} = \frac{\langle \Pi_G O \Pi_G \rangle}{\langle \Pi_G \rangle}. \quad (\text{B3})$$

Since $\Pi_G O \Pi_G$ takes the value 0, 1 and can be 1 if and only if Π_G takes the value 1, we have $(\Pi_G O \Pi_G)^2 = \Pi_G^2 = \Pi_G$. Using this and Eq. (B3), the variance and covariance of the observables are:

$$\begin{aligned} \text{Var}[\Pi_G O \Pi_G] &= \langle (\Pi_G O \Pi_G)^2 \rangle - \langle \Pi_G O \Pi_G \rangle^2 \\ &= \langle \Pi_G \rangle - \langle O_{dir} \rangle^2 \langle \Pi_G \rangle^2 \\ \text{Var}[\Pi_G] &= \langle \Pi_G^2 \rangle - \langle \Pi_G \rangle^2 = \langle \Pi_G \rangle - \langle \Pi_G \rangle^2 \\ \text{Cov}[\Pi_G O \Pi_G, \Pi_G] &= \langle \Pi_G O \Pi_G^2 \rangle - \langle \Pi_G O \Pi_G \rangle \langle \Pi_G \rangle \\ &= \langle O_{dir} \rangle \langle \Pi_G \rangle (1 - \langle \Pi_G \rangle). \end{aligned} \quad (\text{B4})$$

If we can measure all symmetry generators and O in the same circuit run, then in each circuit run, we will obtain one sample for $\Pi_G O \Pi_G$ and one sample for Π_G . Hence, after N circuit runs, our estimation of the symmetry-verified variable is:

$$\overline{O}_{dir} = \frac{\overline{\Pi_G O \Pi_G}}{\overline{\Pi_G}}. \quad (\text{B5})$$

and the corresponding variance can be obtained using Eq. (B2) and Eq. (B4):

$$\begin{aligned} \text{Var}[\overline{O}_{dir}] &= \frac{1}{N \langle \Pi_G \rangle} \left[\left(1 - \langle O_{dir} \rangle^2 \langle \Pi_G \rangle \right) - \langle O_{dir} \rangle^2 (1 - \langle \Pi_G \rangle) \right] \\ &= \frac{1 - \langle O_{dir} \rangle^2}{N \langle \Pi_G \rangle} \end{aligned} \quad (\text{B6})$$

2. Symmetry Expansion

In symmetry expansion, the expectation value is :

$$\langle O_{exp} \rangle = \text{Tr}(O\rho_{\vec{w}}) = \frac{\text{Tr}(O\Gamma_{\vec{w}}\rho)}{\text{Tr}(\Gamma_{\vec{w}}\rho)} = \frac{\langle O\Gamma_{\vec{w}} \rangle}{\langle \Gamma_{\vec{w}} \rangle}. \quad (\text{B7})$$

We will decomposed $O\Gamma_{\vec{w}}$ into:

$$O\Gamma_{\vec{w}} = \frac{\sum_{G \in \mathbb{G}} w_G O G}{\sum_{G' \in \mathbb{G}} w_{G'}}. \quad (\text{B8})$$

Hence, $O\Gamma_{\vec{w}}$ can be sampled by measuring different OG with $\frac{w_G}{\sum_{G' \in \mathbb{G}} w_{G'}}$ probability. $\Gamma_{\vec{w}}$ can be sampled in a similar way by measuring G instead of OG . To estimate $\langle O_{exp} \rangle$, in each circuit run we will measure the observable O along with the symmetry operator G with probability $\frac{w_G}{\sum_{G' \in \mathbb{G}} w_{G'}}$. They can be composed to obtain OG

and G , giving us one sample each to the variable $O\Gamma_{\vec{w}}$ and $\Gamma_{\vec{w}}$. Note that sampling in this way will means that $O\Gamma_{\vec{w}}$ and $\Gamma_{\vec{w}}$ are variables that return ± 1 for each sample. Hence, we have $(O\Gamma_{\vec{w}})^2 = \Gamma_{\vec{w}}^2 = 1$, and also $O\Gamma_{\vec{w}}\Gamma_{\vec{w}} = O\Gamma_{\vec{w}}^2 = O$. Using these and Eq. (B7), the variance and covariance of the observables are:

$$\begin{aligned} \text{Var}[O\Gamma_{\vec{w}}] &= \langle (O\Gamma_{\vec{w}})^2 \rangle - \langle O\Gamma_{\vec{w}} \rangle^2 = 1 - \langle O\Gamma_{\vec{w}} \rangle^2 \\ &= 1 - \langle O_{exp} \rangle^2 \langle \Gamma_{\vec{w}} \rangle^2 \\ \text{Var}[\Gamma_{\vec{w}}] &= \langle \Gamma_{\vec{w}}^2 \rangle - \langle \Gamma_{\vec{w}} \rangle^2 = 1 - \langle \Gamma_{\vec{w}} \rangle^2 \\ \text{Cov}[O\Gamma_{\vec{w}}, \Gamma_{\vec{w}}] &= \langle O\Gamma_{\vec{w}}\Gamma_{\vec{w}} \rangle - \langle O\Gamma_{\vec{w}} \rangle \langle \Gamma_{\vec{w}} \rangle \\ &= \langle O \rangle - \langle O_{exp} \rangle \langle \Gamma_{\vec{w}} \rangle^2. \end{aligned} \quad (\text{B9})$$

When we sample in the way outlined above, for each circuit run, we get one sample for $O\Gamma_{\vec{w}}$ and one sample for $\Gamma_{\vec{w}}$ just like in the direct verification case, it is just that these two variables are different random variable now. Hence, after N circuit runs, our estimation of the symmetry-expanded variable is:

$$\overline{O}_{exp} = \frac{\overline{O\Gamma_{\vec{w}}}}{\overline{\Gamma_{\vec{w}}}} \quad (\text{B10})$$

and the corresponding variance can be obtained using Eq. (B2) and Eq. (B9):

$$\begin{aligned} \text{Var}[\overline{O}_{exp}] &= \frac{1}{N \langle \Gamma_{\vec{w}} \rangle^2} \left[1 - \langle O_{exp} \rangle^2 \langle \Gamma_{\vec{w}} \rangle^2 \right. \\ &\quad \left. - 2 \langle O_{exp} \rangle \left(\langle O \rangle - \langle O_{exp} \rangle \langle \Gamma_{\vec{w}} \rangle^2 \right) + \langle O_{exp} \rangle^2 \left(1 - \langle \Gamma_{\vec{w}} \rangle^2 \right) \right] \\ &= \frac{1 - 2 \langle O_{exp} \rangle \langle O \rangle + \langle O_{exp} \rangle^2}{N \langle \Gamma_{\vec{w}} \rangle^2}. \end{aligned}$$

3. Comparison

When we directly sample from the noisy circuit, after N circuit runs, the variance in the estimator of O is:

$$\text{Var}[\overline{O}] = \frac{\langle O^2 \rangle - \langle O \rangle^2}{N} = \frac{1 - \langle O \rangle^2}{N}, \quad (\text{B11})$$

which is upper-bounded by $\frac{1}{N}$. Compared to the upper-bounds of the variance using symmetry verification and symmetry expansion in Eq. (B6) and Eq. (B11), the sampling cost factors are given by:

- Direct Symmetry Verification:

$$C_{dir} = \frac{\text{Var}[\overline{O}_{dir}]}{\text{Var}[\overline{O}]} \sim \langle \Pi_G \rangle^{-1} \equiv \langle \Gamma_I \rangle^{-1} \quad (\text{B12})$$

- Symmetry Expansion (including post-processing symmetry verification):

$$C_{\vec{w}} = \frac{\text{Var}[\overline{O}_{exp}]}{\text{Var}[\overline{O}]} \sim \langle \Gamma_{\vec{w}} \rangle^{-2}. \quad (\text{B13})$$

Appendix C: Virtual Distillation

Here we will revisit the virtual distillation protocol introduced in Refs. [11, 12] from the perspective of symmetry expansion. Suppose we are interested in the ideal state $|\phi_0\rangle$. We can prepare M copies of it: $|\psi_0\rangle = |\phi_0\rangle^{\otimes M}$, such that it is invariant under any permutation between the copies. Hence, its symmetry group is the permutation group of M elements, denoting as \mathbb{S}_M . The projection operator into the subspace stabilised by \mathbb{S}_M is simply:

$$\Pi_M = \frac{1}{|\mathbb{S}_M|} \sum_{S \in \mathbb{S}_M} S = \frac{1}{M!} \sum_{S \in \mathbb{S}_M} S. \quad (\text{C1})$$

In reality, we have M copies of the noisy state $\rho = \sigma^{\otimes M}$ instead. Hence, we can implement symmetry verification using the permutation group to project the noisy state into the symmetry subspace defined by Eq. (C1) [13–15].

Since the M copies of the noisy state are identical, we know that $\rho = \sigma^{\otimes M}$ commute with all $S \in \mathbb{S}_M$, and thus commute with Π_M . Hence, the effective state we have after the symmetry verification is:

$$\rho_{\text{sym}} = \frac{\Pi_M \rho \Pi_M}{\text{Tr}(\Pi_M \rho \Pi_M)} = \frac{\Pi_M \rho}{\text{Tr}(\Pi_M \rho)}. \quad (\text{C2})$$

This is a special case of the symmetry expanded state in Eq. (10) with $\mathbb{G} = \mathbb{S}_M$ and uniform weights.

From here on, our discussion will deviate from the main text since in virtual distillation, we only care about the observable on *the first copy*. If we observe an observable O_1 on the first copy of the symmetry-expanded state, we have:

$$\text{Tr}(O_1 \rho_{\vec{w}}) = \frac{\text{Tr}(O_1 \Gamma_{\vec{w}} \rho)}{\text{Tr}(\Gamma_{\vec{w}} \rho)} = \frac{\sum_{S \in \mathbb{S}_M} w_S \text{Tr}(O_1 S \rho)}{\sum_{S \in \mathbb{S}_M} w_S \text{Tr}(S \rho)}.$$

By direct calculation, we have

$$\text{Tr}(O_1 S \rho) = \text{Tr}(O_1 S \sigma^{\otimes M}) = \text{Tr}(O_1 \sigma^{m_S})$$

where we use m_S to denote the order of the cycle that copy 1 belongs to in the cyclic representation of the permutation operator S . Hence, here using the structure of our problem, we have successfully identified sets of permutation operators within which all symmetry operators are equivalent for the purpose of being the components of symmetry expansion to observe O_1 . Each set here contains permutation operators that have 1 in a cycle of the same given order m . Let us define C_m as the cyclic permutation operator acting on the *first* m copies, which is one of the operators in the set that has 1 in an m -cycle, then we simply have:

$$\text{Tr}(O_1 S \rho) = \text{Tr}(O_1 C_{m_S} \rho) \quad \forall S \in \mathbb{S}_M.$$

Hence, our symmetry expansion operator only needs to have one element from each equivalent class, which are

just C_m of different m . It can be rewritten as:

$$\Gamma_{\vec{w}} = \frac{\sum_{m=1}^M w_m C_m}{\sum_{m=1}^M w_m},$$

and the symmetry projected observable is simply:

$$\frac{\text{Tr}(O_1 \Gamma_{\vec{w}} \rho)}{\text{Tr}(\Gamma_{\vec{w}} \rho)} = \frac{\sum_{m=1}^M w_m \text{Tr}(O_1 \sigma^m)}{\sum_{m=1}^M w_m \text{Tr}(\sigma^m)}$$

Now if O_1 is the ideal state $\sigma_0 = |\phi_0\rangle \langle \phi_0|$, we then have fidelity of the symmetry expanded state against the ideal state of the first copy being:

$$F = \frac{\text{Tr}(\sigma_0 \Gamma_{\vec{w}} \rho)}{\text{Tr}(\Gamma_{\vec{w}} \rho)} = \frac{\sum_{m=1}^M w_m \text{Tr}(\sigma_0 \sigma^m)}{\sum_{m=1}^M w_m \text{Tr}(\sigma^m)}$$

We can rewrite it as

$$F_{\vec{p}} = \sum_{m=1}^M p_m \frac{\text{Tr}(\sigma_0 \sigma^m)}{\text{Tr}(\sigma^m)}$$

where

$$p_m = \frac{w_m \text{Tr}(\sigma^m)}{\sum_{m=1}^M w_m \text{Tr}(\sigma^m)}.$$

i.e. $F_{\vec{p}}$ is a weighted sum of $\frac{\text{Tr}(\sigma_0 \sigma^m)}{\text{Tr}(\sigma^m)}$. Therefore, we have:

$$\max_{\vec{p}} F_{\vec{p}} \leq \max_m \frac{\text{Tr}(\sigma_0 \sigma^m)}{\text{Tr}(\sigma^m)}$$

From Refs. [11, 12] we see that:

$$\max_m \frac{\text{Tr}(\sigma_0 \sigma^m)}{\text{Tr}(\sigma^m)} = \frac{\text{Tr}(\sigma_0 \sigma^M)}{\text{Tr}(\sigma^M)},$$

which in terms implies the \vec{w} that maximise $F_{\vec{p}}$ is the one with $w_M = 1$ and all other $w_m = 0$.

Hence, the optimal symmetry-expanded density operator is:

$$\frac{C_M \rho}{\text{Tr}(C_M \rho)}$$

which is just the density operator used for virtual distillation in Refs. [11, 12]. Symmetry expansion in this case was shown to be able to reduce the infidelity exponentially with increase of M while symmetry verification can only reduce the infidelity linearly with increase of M .

Besides the performance improvement, using symmetry expansion over symmetry verification in this case and more generally for non-abelian symmetry group also has advantages in terms of circuit implementation. For symmetry expansion, we only require measuring one symmetry operator along with the observable in the same circuit run. If the expectation value of the symmetry operator is real, then no ancilla and complicated long-range gates between ancilla and data are required for symmetry expansion. In the example of virtual distillation, such circuits are constructed in Ref. [12].

Appendix D: Fraction of Detectable Errors in Fermi-Hubbard Simulation

Similar discussion can be found in Ref. [19]. Since the quantum states in between our two-component gates have well-defined G_{tot} , any Pauli errors that anti-commute with G_{tot} will be flip the G_{tot} value and get detected. Similarly for G_{\uparrow} and G_{\downarrow} .

As discussed in Section V, our circuit only consists of two-qubit gate affected by two-qubit depolarising errors and G_{tot} is simply the tensor product of Z acting on all qubits. Hence, out of the 15 two-qubit Pauli errors, only the error components generated by $\{Z_1, Z_2, X_1 X_2\}$ (excluding identity) are undetectable by G_{tot} . Hence, 8 out of 15 Pauli error components are detectable by G_{tot} , which means

$$f_{G_{tot}} = \frac{8}{15}.$$

Now to calculate the fraction of errors detectable by G_{\uparrow} , we need to divide our two-qubit gates into three types:

- Gates acting across both spin spaces:

Suppose qubit 1 is in spin up and qubit 2 is in spin down, then the two-qubit error components that are undetectable by G_{\uparrow} is generated by

$\{Z_1, Z_2, X_2\}$, excluding identity. Hence, for the errors in these gates, the fraction of error detectable by G_{\uparrow} is $8/15$.

- Gates acting within the spin-up subspace:

Similar to our discussion of G_{tot} , $8/15$ of the errors are detectable by G_{\uparrow}

- Gates acting within the spin-down subspace:

All errors are undetectable by G_{\uparrow} .

Since our circuit consists of alternating layers of gates acting across the spin subspaces and acting within the spin subspaces, we should expect roughly $\frac{1}{2}$ of the gates are acting across different spin spaces, roughly $\frac{1}{4}$ of the gates are acting within the spin-up subspace and roughly $\frac{1}{4}$ within the spin down subspace. Hence, the total fraction of errors detectable by G_{\uparrow} is thus:

$$f_{G_{\uparrow}} \sim \frac{1}{2} \times \frac{8}{15} + \frac{1}{4} \times \frac{8}{15} + \frac{1}{4} \times 0 = \frac{2}{5}.$$

Similarly we also have:

$$f_{G_{\downarrow}} \sim \frac{2}{5}.$$

-
- [1] F. Arute, K. Arya, R. Babbush, D. Bacon, J. C. Bardin, R. Barends, R. Biswas, S. Boixo, F. G. S. L. Brandao, D. A. Buell, B. Burkett, Y. Chen, Z. Chen, B. Chiaro, R. Collins, W. Courtney, A. Dunsworth, E. Farhi, B. Foxen, A. Fowler, C. Gidney, M. Giustina, R. Graff, K. Guerin, S. Habegger, M. P. Harrigan, M. J. Hartmann, A. Ho, M. Hoffmann, T. Huang, T. S. Humble, S. V. Isakov, E. Jeffrey, Z. Jiang, D. Kafri, K. Kechedzhi, J. Kelly, P. V. Klimov, S. Knysh, A. Korotkov, F. Kostritsa, D. Landhuis, M. Lindmark, E. Lucero, D. Lyakh, S. Mandrà, J. R. McClean, M. McEwen, A. Megrant, X. Mi, K. Michielsen, M. Mohseni, J. Mutus, O. Naaman, M. Neeley, C. Neill, M. Y. Niu, E. Ostby, A. Petukhov, J. C. Platt, C. Quintana, E. G. Rieffel, P. Roushan, N. C. Rubin, D. Sank, K. J. Satzinger, V. Smelyanskiy, K. J. Sung, M. D. Trevithick, A. Vainsencher, B. Villalonga, T. White, Z. J. Yao, P. Yeh, A. Zalcman, H. Neven, and J. M. Martinis, Quantum supremacy using a programmable superconducting processor, *Nature* **574**, 505 (2019).
 - [2] H.-S. Zhong, H. Wang, Y.-H. Deng, M.-C. Chen, L.-C. Peng, Y.-H. Luo, J. Qin, D. Wu, X. Ding, Y. Hu, P. Hu, X.-Y. Yang, W.-J. Zhang, H. Li, Y. Li, X. Jiang, L. Gan, G. Yang, L. You, Z. Wang, L. Li, N.-L. Liu, C.-Y. Lu, and J.-W. Pan, Quantum computational advantage using photons, *Science* **370**, 1460 (2020).
 - [3] K. Temme, S. Bravyi, and J. M. Gambetta, Error Mitigation for Short-Depth Quantum Circuits, *Physical Review Letters* **119**, 180509 (2017).
 - [4] S. Endo, S. C. Benjamin, and Y. Li, Practical Quantum Error Mitigation for Near-Future Applications, *Physical Review X* **8**, 031027 (2018).
 - [5] Z. Cai, Multi-exponential Error Extrapolation and Combining Error Mitigation Techniques for NISQ Applications, *arXiv:2007.01265 [quant-ph]* (2020).
 - [6] S. Endo, Z. Cai, S. C. Benjamin, and X. Yuan, Hybrid quantum-classical algorithms and quantum error mitigation, *arXiv:2011.01382 [quant-ph]* (2020).
 - [7] X. Bonet-Monroig, R. Sagastizabal, M. Singh, and T. E. O'Brien, Low-cost error mitigation by symmetry verification, *Physical Review A* **98**, 062339 (2018).
 - [8] S. McArdle, X. Yuan, and S. Benjamin, Error-Mitigated Digital Quantum Simulation, *Physical Review Letters* **122**, 180501 (2019).
 - [9] J. R. McClean, M. E. Kimchi-Schwartz, J. Carter, and W. A. de Jong, Hybrid quantum-classical hierarchy for mitigation of decoherence and determination of excited states, *Physical Review A* **95**, 042308 (2017).
 - [10] J. R. McClean, Z. Jiang, N. C. Rubin, R. Babbush, and H. Neven, Decoding quantum errors with subspace expansions, *Nature Communications* **11**, 636 (2020).
 - [11] B. Koczor, Exponential Error Suppression for Near-Term Quantum Devices, *arXiv:2011.05942 [quant-ph]* (2020).
 - [12] W. J. Huggins, S. McArdle, T. E. O'Brien, J. Lee, N. C. Rubin, S. Boixo, K. B. Whaley, R. Babbush, and J. R. McClean, Virtual Distillation for Quantum Error Mitigation, *arXiv:2011.07064 [quant-ph]* (2020).
 - [13] A. Berthiaume, D. Deutsch, and R. Jozsa, The stabilisation of quantum computations, in *Proceedings Workshop on Physics and Computation. PhysComp '94* (1994) pp.

- 60–62.
- [14] A. Barenco, A. Berthiaume, D. Deutsch, A. Ekert, R. Jozsa, and C. Macchiavello, Stabilization of Quantum Computations by Symmetrization, *SIAM Journal on Computing* **26**, 1541 (1997).
 - [15] A. Peres, Error Symmetrization in Quantum Computers, *International Journal of Theoretical Physics* **38**, 799 (1999).
 - [16] W.-K. Tung, *Group Theory in Physics: An Introduction to Symmetry Principles, Group Representations, and Special Functions in Classical and Quantum Physics* (WORLD SCIENTIFIC, 1985).
 - [17] A. Jena, S. Genin, and M. Mosca, Pauli Partitioning with Respect to Gate Sets, [arXiv:1907.07859 \[quant-ph\]](https://arxiv.org/abs/1907.07859) (2019).
 - [18] W. J. Huggins, J. McClean, N. Rubin, Z. Jiang, N. Wiebe, K. B. Whaley, and R. Babbush, Efficient and Noise Resilient Measurements for Quantum Chemistry on Near-Term Quantum Computers, [arXiv:1907.13117 \[physics, physics:quant-ph\]](https://arxiv.org/abs/1907.13117) (2019).
 - [19] Z. Cai, Resource Estimation for Quantum Variational Simulations of the Hubbard Model, *Physical Review Applied* **14**, 014059 (2020).
 - [20] A. Strikis, D. Qin, Y. Chen, S. C. Benjamin, and Y. Li, Learning-based quantum error mitigation, [arXiv:2005.07601 \[quant-ph\]](https://arxiv.org/abs/2005.07601) (2020).
 - [21] K. Mitarai and K. Fujii, Methodology for replacing indirect measurements with direct measurements, *Physical Review Research* **1**, 013006 (2019).
 - [22] Z. Cai, X. Xu, and S. C. Benjamin, Mitigating coherent noise using Pauli conjugation, *npj Quantum Information* **6**, 1 (2020).
 - [23] T. Jones and S. C. Benjamin, QuESTlink – Mathematica embiggened by a hardware-optimised quantum emulator, *Quantum Science and Technology* **10.1088/2058-9565/ab8506** (2020).
 - [24] T. Jones, A. Brown, I. Bush, and S. C. Benjamin, QuEST and High Performance Simulation of Quantum Computers, *Scientific Reports* **9**, 1 (2019).